Polarization-Phase Mapping of the Optically Anisotropic Component of Biological Tissues in the Differential Diagnosis of Sepsis

I.Oliinyk[1)], Yu. Solovey[1)], V.Polovyi[1)], A. Dubolazov[2)], Yu.Ushenko[2)], I. Soltys[2)], A. Motrich[2)]

[1)] *Bukovinian State Medical University, 3 Theatral Sq., Chernivtsi, Ukraine, 58000*
[2)] *Chernivtsi National University, 2 Kotsiubynskyi Str., Chernivtsi, Ukraine, 58012*
a.dubolazov@chnu.edu.ua

ABSTRACT

A new digital technique of objective differential diagnosis of the septic process severity was developed and tested experimentally by polarization-phase mapping of microscopic images of histological sections of the liver of laboratory rats based on statistical and information analysis of phase shift distributions.

Keywords: polarization, Jones matrix, diagnosis, biological tissue.

1. Introduction

In matrix form, the transformation of the complex amplitude by an optically anisotropic biological layer can be written as the following equation [1-5]

$$U = \{P\}\{D\}\{A\}U_0 . \tag{1}$$

Here $\{P\}$ - Jones matrix of polarizer; $\{D\}$ - the Jones matrix of an optically uniaxial birefringent biological crystal; $\{A\}$ - Jones matrix of analyzer; U_0 - Jones vector of the incident laser wave; U - Jones vector of converted laser wave. Under these conditions, the expressions for partial vectors and Jones matrices take the form

$$\begin{cases} \{A\} = \begin{Vmatrix} 1 & -1 \\ -1 & 1 \end{Vmatrix}; \\ \{D\} = \begin{Vmatrix} d_{11} & d_{12} \\ d_{21} & d_{22} \end{Vmatrix} = \begin{Vmatrix} \cos^2\rho + \sin^2\rho\exp(-i\delta); & \cos\rho\sin\rho(1-\exp(-i\delta)); \\ \cos\rho\sin\rho(1-\exp(-i\delta)); & \sin^2\rho + \cos^2\rho\exp(-i\delta) \end{Vmatrix}; \\ \{P\} = \begin{Vmatrix} 1 & 1 \\ 1 & 1 \end{Vmatrix}; \\ U_0 = \begin{pmatrix} U_{0x} \\ U_{0y}\exp(-i\delta_0) \end{pmatrix} = \begin{pmatrix} 1 \\ 1 \end{pmatrix}; \\ U = \begin{pmatrix} U_x \\ U_y\exp(-i\delta) \end{pmatrix}. \end{cases} \tag{2}$$

The resulting Jones vector, taking into account expressions (1) and (2), is determined by the following equation

$$U = 0.25\begin{Vmatrix} 1 & -1 \\ -1 & 1 \end{Vmatrix}\begin{Vmatrix} \cos^2\rho + \sin^2\rho\exp[-i\delta] & \cos\rho\sin\rho\{1-\exp[-i\delta]\} \\ \cos\rho\sin\rho\{1-\exp[-i\delta]\} & \sin^2\rho + \cos^2\rho\exp[-i\delta] \end{Vmatrix} \times\times \begin{Vmatrix} 1 & 1 \\ 1 & 1 \end{Vmatrix}\begin{pmatrix} 1 \\ 1 \end{pmatrix}. \tag{3}$$

For direct experimental determination of the coordinate distribution of phase shifts $\delta(x,y)$ between orthogonal amplitude components at the points $r \leftrightarrow (x,y)$ of the laser image of the optically anisotropic layer, it was proposed [2] to place its sample between two crossed polarizing filters — quarter-wave plates and polarizers, the transmission planes of which are angles with axes of maximum speed $+45^0$ and -45^0.
The amplitude E of the converted laser beam in such an experimental arrangement is determined by the equation

$$E = 0.25\{A\}\{\Phi_2\}\{M\}\{\Phi_1\}\{P\}E_0 = 0.25\begin{Vmatrix} 1 & -1 \\ -1 & 1 \end{Vmatrix}\begin{Vmatrix} i & 0 \\ 0 & 1 \end{Vmatrix}\times$$
$$\times\begin{Vmatrix} \cos^2\rho + \sin^2\rho\exp[-i\delta] & \cos\rho\sin\rho\{1-\exp[-i\delta]\} \\ \cos\rho\sin\rho\{1-\exp[-i\delta]\} & \sin^2\rho + \cos^2\rho\exp[-i\delta] \end{Vmatrix}\times\begin{Vmatrix} 1 & 0 \\ 0 & i \end{Vmatrix}\begin{Vmatrix} 1 & 1 \\ 1 & 1 \end{Vmatrix}\begin{pmatrix} 1 \\ 1 \end{pmatrix}. \quad (4)$$

Here $\{\Phi_1\}$, $\{\Phi_2\}$ – quarter-wave Jones matrices.
The solution to the matrix equation (4) is the intensity value $I(\delta)$ at the point with the coordinates (x,y) of the laser image of the biological crystal

$$I(\delta) = EE^{\otimes} = I_0 \sin^2\left[\delta/2\right]. \quad (5)$$

2. Methods of phase metric mapping of microscopic images of biological objects

In Fig. 1 presents a structural and logical scheme and method of polarization-phase microscopy of histological sections of internal organs and blood films of laboratory rats.

Block of coherent irradiation of histological sections of internal organs and blood films of laboratory rats
Block for forming circular polarization of the laser probe
Object unit for placing samples of biological objects
The unit for forming a microscopic image of samples of biological objects
Block of polarization-phase analysis of microscopic images of biological objects
Block of digital registration of polarization-phase microscopic images of biological objects
Computer processor for calculating the phases of microscopic images of biological objects
Computer processor for statistical analysis of the phase distribution of microscopic images of biological objects

Fig. 1. Structural and logical scheme and methods of polarization-phase microscopy of biological objects

Experimental measurement of the coordinate distributions of the magnitude of the phase shifts was performed in the location of the laser micropolarimeter, the optical scheme of which is given in scientific papers [1-7] and is presented in Fig. 2.

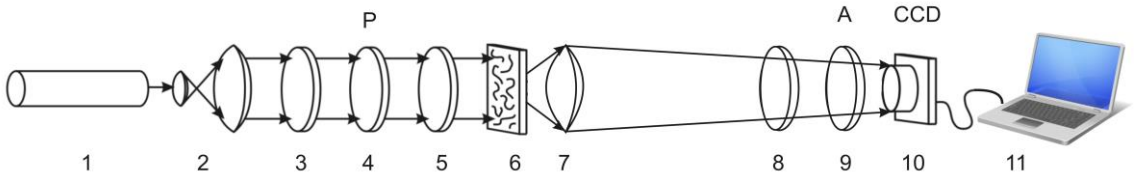

Fig. 2. Optical scheme of the micropolarimeter

Here:
1 - He-Ne laser;
2 - collimator;
3, 5, 8 - quarter-wave plates;
4, 9 - polarizer and analyzer, respectively;
6 - object of study;
7 - microlens;
10 - CCD camera;
11 - personal computer.

Irradiation was performed with a parallel beam (Ø = μm) of He-Ne laser (λ = 0.6328 μm) [1]. Polarizing filter (quarter-wave plate 3, 5 (manufacturer - Achromatic True Zero-Order Waveplate) and polarizer 4 (manufacturer - B + W Kaesemann XS-Pro Polarizer MRC Nano)) formed a right circularly polarized laser beam - probe.
Images of biological preparations of rats 6 were projected using a polarizing microlens 7 (manufacturer - Nikon CFI Achromat P, focal length - 30mm, numerical aperture - 0.1, magnification - 4x) in the plane of the light-sensitive area of the CCD camera 10 (The Imaging Source DMK 41AU02 .AS, monochrome 1/2 "CCD, Sony ICX205AL (progressive scan); resolution - 1280x960; light-sensitive pad size - 7600x6200μm; sensitivity - 0.05 lx; dynamic range - 8 bit, SNR - 9 bit), light-sensitive pad which contains pixels.
By rotating the transmission axis of the analyzer 9 (manufacturer - B + W Kaesemann XS-Pro Polarizer MRC Nano) at an angle $\Theta = -45^0$ relative to the axis of the highest speed of the quarter-wave plate 8, the transmission conditions of the left circularly polarized states were formed.

3. Experimental results and their discussion

In a series of fragments of Fig. 3 - Fig. 4 are presented phase maps ((1), (3)) and histograms of the magnitude of phase shifts distributions (2), (4), which are defined for digital microscopic images of blood polycrystalline films of rats from group 1 (Fig. 3, fragments), (2)), groups 2.1 (Fig. 3, fragments (3), (4)), groups 3.1 (Fig. 4, fragments (1), (2)) and groups 4.1 (Fig.4, fragments (3), (4))[8-11].

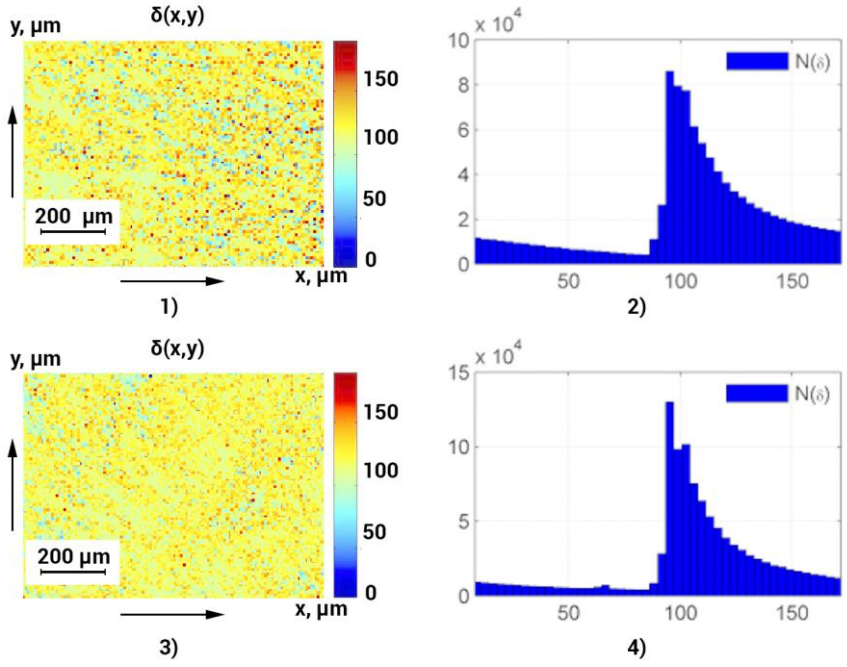

Fig. 3. Phase maps (fragments (1), (3)) and histograms (fragments (2), (4)) of distributions of the magnitude of phase shifts at the points of microscopic images of polycrystalline blood films of rats from group 2.1 and group 2.2

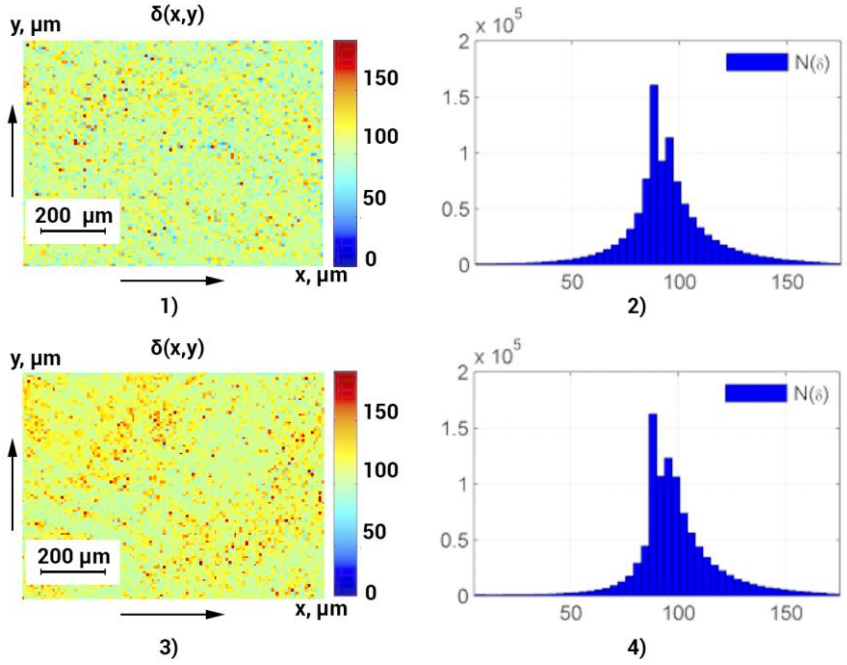

Fig. 4. Phase maps (fragments (1), (3)) and histograms (fragments (2), (4)) of distributions of the magnitude of phase shifts at the points of microscopic images of polycrystalline films of rat blood from group 3.1 and group 4.1.

Comparative analysis of the obtained data of polarization-phase microscopy of polycrystalline blood films revealed:

- coordinate and statistical inhomogeneity of distributions of the magnitude of phase shifts, which are formed by the polycrystalline component of the samples from all groups;
- histograms of distributions of the magnitude of phase shifts (fragments (2), (4)) at points of microscopic images are characterized by different half-widths of the scatter of phase values.
- individual topographic and statistical structure of phase maps (fragments (1), (3)) of digital microscopic images of polycrystalline blood films of rats of all groups;
- reduction of the average and range of phase scatter in the phase maps of microscopic images of polycrystalline films of rat blood with increasing severity of the septic process (fragments (2), (4)) Fig. 3 and fig. 4, respectively).

The results of the statistical analysis of phase maps are shown in table 1.

Table 1 Statistical parameters of phase maps of histological sections of lung tissue

Groups	**Group 1 Intact** $(n=39)$	**Group 2 Sepsis (easy)** $(n=39)$		**Group 2 Sepsis (average)** $(n=39)$	
Duration	**0 hours**	**2.1 (12 hours)**	**2.2 (48 hours)**	**3.1 (12 hours)**	**3.2 (48 hours)**
Average, S	$1{,}39 \pm 0{,}067$	$1{,}12 \pm 0{,}047$	$0{,}94 \pm 0{,}041$	$0{,}75 \pm 0{,}032$	$0{,}62 \pm 0{,}027$
Dispersion, D	$1{,}22 \pm 0{,}058$	$1{,}08 \pm 0{,}044$	$0{,}85 \pm 0{,}038$	$0{,}71 \pm 0{,}032$	$0{,}55 \pm 0{,}024$
Asymmetry, A	$0{,}91 \pm 0{,}041$	$1{,}19 \pm 0{,}052$	$1{,}31 \pm 0{,}062$	$1{,}52 \pm 0{,}071$	$1{,}71 \pm 0{,}083$
Excess, E	$2{,}03 \pm 0{,}099$	$1{,}76 \pm 0{,}084$	$1{,}51 \pm 0{,}077$	$1{,}29 \pm 0{,}059$	$1{,}03 \pm 0{,}043$

1. The central statistical moment of the 1st order:
   - the average group value of the average S within the set of representative samples of "group 1 - group 4" rats decreases from 1.39 to 0.43;
   - intergroup differences - statistically significant ($p_{1\div4}$, $p_{2\div3}$, $p_{3\div4}$, $p_{2\div4}$ p 0,05);
2. The central statistical moment of the 2nd order:
   - the average group value of the dispersion D within the set of representative samples "group 1 - group 4" decreases from 1.22 to 0.36;
   - intergroup differences - statistically significant for all groups ($p_{1\div4}$, $p_{2\div3}$, $p_{3\div4}$, $p_{2\div4}$ p 0,05);
3. The central statistical moment of the 3rd order:
   - the average group value of the asymmetry within the set of representative samples "group 1 - group 4" grows in the range from 0.91 to 2.01;
   - intergroup differences - statistically significant for all groups ($p_{1\div4}$, $p_{2\div3}$, $p_{3\div4}$, $p_{2\div4}$ p 0,05)
4. The central statistical moment of the 4th order: :
   - the average group value of the excecss E within the set of representative samples "group 1 - group 4" decreases from 2.03 to 0.83;
   - intergroup differences - statistically significant ($p_{1\div4}$, $p_{2\div3}$, $p_{3\div4}$, $p_{2\div4}$ p 0,05).

Table 2 presents the results of determining the balanced accuracy of the method of phase mapping of microscopic images of histological sections of the lung tissue of healthy and sick sepsis rats.

Table 2 Balanced accuracy of differential diagnosis of sepsis severity by phase maps of histological sections of lung tissue

Groups	"1 – (2,3,4)"	"2-3"
Average, S	79,5	76,9
Dispersion, D	78,2	76,9
Asymmetry, A	93,6	92,3
Excess, E	91	92,3

Conclusions

The following ranges of maximum balanced accuracy were identified:

- intact - patients **"1 - (2,3)"** - excellent quality $Ac(A.E) = 91\% - 93{,}6\%$;
- easy - average grade **"2-3"** - excellent quality $Ac(A.E) = 92{,}3\%$.

References

[1]. Statistical, Correlation and Topological Approaches in Diagnostics of the Structure and Physiological State of Birefringent Biological Tissues / O. V. Angelsky, A. G. Ushenko, Yu. A. Ushenko, V. P. Pishak, A. P. Peresunko // Handbook of Photonics for Biomedical Science; Ed. by Valery V. Tuchin – London. : CRC Press. – 2010. – P. 283-322.

[2]. Diagnostics of Structure and Physiological State of Birefringent Biological Tissues: Statistical, Correlation and Topological Approaches / Y. A. Ushenko, T. M. Boychuk, V. T. Bachynsky, O. P. Mincer // Handbook of Coherent-Domain Optical Methods. – New York : Springer Science+Business Media – 2013. – P. 107-148.

[3]. Ushenko, A.G., Dubolazov, O.V., Bachynsky, V.T., Peresunko, A.P., Vanchulyak, O.Y., "On the feasibilities of using the wavelet analysis of mueller matrix images of biological crystals," (2010) Advances in Optical Technologies, 162832.

[4]. Zabolotna, N.I., Wojcik, W., Pavlov, S.V., Ushenko, O.G., Suleimenov, B., "Diagnostics of pathologically changed birefringent networks by means of phase Mueller matrix tomography," (2013) Proceedings of SPIE - The International Society for Optical Engineering, 8698, 86980.

[5]. Ushenko, A.G., "Correlation Processing and Wavelet Analysis of Polarization Images of Biological Tissues," (2001) Optics and Spectroscopy (English translation of Optika i Spektroskopiya), 91 (5), pp. 773-778.

[6]. Ushenko, A.G., Ermolenko, S.B., Burkovets, D.N., Ushenko, Yu.A., "Polarization microstructure of laser radiation scattered by optically active biotissues," (1999) Optika i Spektroskopiya, 87 (3), pp. 470-474.

[7]. Ushenko, A.G., Dubolazov, A.V., Ushenko, V.A., Novakovskaya, O.Y., "Statistical analysis of polarization-inhomogeneous Fourier spectra of laser radiation scattered by human skin in the tasks of differentiation of benign and malignant formations," (2016) Journal of Biomedical Optics, 21 (7), 071110.
[8]. Bekshaev AY, Angelsky OV, Sviridova SV, Zenkova CY. Mechanical action of inhomogeneously polarized optical fields and detection of the internal energy flows. Adv Opt Technol 2011.
[9]. Angelsky, O. V., Maksimyak, P. P., &Perun, T. O. (1993). Optical correlation method for measuring spatial complexity in optical fields. Optics Letters, 18(2), 90-92.
[10]. Angelsky, O. V., Bekshaev, A. Y. A., Maksimyak, P. P., Maksimyak, A. P., & Hanson, S. G. (2018). Low-temperature laser-stimulated controllable generation of micro-bubbles in a water suspension of absorptive colloid particles. Optics Express, 26(11), 13995-14009.
[11]. Angelsky, O. V. (2007). Optical correlation techniques and applications. Optical correlation techniques and applications (pp. 1-270).